# MODULATED AND LOCALISED STATES IN A FINITE DOMAIN

J. H. P. DAWES*

**Abstract.** A subcritical pattern-forming (Turing) instability of a uniform state, in an infinite domain, produces two branches of spatially localised states that bifurcate from the pattern-forming instability along with a uniform spatially-periodic pattern. In this paper we demonstrate that branches of localised states persist as strongly amplitude-modulated patterns in large, but finite, domains with periodic boundary conditions. Our analysis is carried out for a model Swift–Hohenberg equation with a cubic–quintic nonlinearity. If the domain size exceeds a critical value, modulated states appear in secondary bifurcations from the primary branch of spatially-periodic solutions. Multiple-scales analysis indicates that these secondary bifurcations occur close to the primary instability, and close to the saddle-node bifurcation on the spatially-periodic solution branch.

As the domain size increases, extra 'turns' on the snaking curve arise through a repeating sequence of saddle-node bifurcations and mode interactions between periodic patterns of nearby wavenumbers. With periodic boundary conditions, the crosslinks in the 'snakes and ladders' structure identified by previous authors in the infinite domain case also persist in finite domains. However, the imposition of either Dirichlet or Neumann boundary conditions preserves one of the two branches of localised states that exist in the infinite domain case and causes the other to fragment.

**Key words.** Homoclinic snaking, pattern formation, bifurcation

**AMS subject classifications.** 76E25, 34E13, 35B32

**1. Introduction.** Localised states have been observed, both experimentally and in numerical simulations, in a wide variety of pattern-forming systems. Well-known examples of experimental systems in which localised states appear include nonlinear optics [37, 1, 7], the buckling of elastic beams [8, 21], filamentary gas discharge systems [35] and many fluid mechanical situations [32, 33, 2, 3, 15, 28, 31].

In one spatial dimension, generally speaking, localised states arise as a result of bistability between a trivial, homogeneous background state and an 'active', patterned, state. In mathematical terms, localised states have been proved to arise generically near subcritical pattern-forming instabilities [22, 38, 14] and their existence can be investigated through analysis of both a 'spatial dynamical system' and through asymptotic multiple-scales arguments [11, 12]. The latter has been extended substantially from the usual leading-order calculation to investigate exponentially small terms that delimit the exact region of existence of the localised states [24, 13].

In an infinite one-dimensional domain, 'homoclinic snaking' is the term used to describe the typical bifurcation diagram that organises the localised states. Stable localised patches of pattern coexist with a stable trivial state due to 'pinning' of the front between the pattern and the trivial state caused by the influence of the local phase of the pattern. This pinning effect, which causes the localised state to persist over an open interval of parameter values, was identified by Pomeau [29] and many authors since: [5, 27, 34, 14]. At a mathematical level, the subcritical pattern-forming instability in which these localised states bifurcate corresponds to a reversible $1:1$ resonance point (also known as a Hamiltonian–Hopf bifurcation) for the spatial dynamical system generated by looking for steady states of a fourth-order PDE [22, 38]. Despite much recent work on aspects of localised states in many contexts, many unresolved issues remain [23], not least the provision of mathematical proofs of numerical results. Recent progress on the mathematical side has been made by [4].

*Department of Mathematical Sciences, University of Bath, Claverton Down, Bath BA2 7AY

In two dimensions the situation is more complicated. Snaking diagrams for localised patches of a hexagonal pattern, for the quadratic-cubic Swift–Hohenberg equation, were investigated in detail by Lloyd et al [25]. Recent results by Lloyd and Sandstede [26] for axisymmetric structures indicate that localised rings bifurcate at small amplitude near a subcritical Turing instability, but that localised spots bifurcate regardless of whether the Turing instability is subcritical or supercritical.

In this paper, in contrast to much existing work, we consider the effect on the snaking bifurcation structure of a finite spatial domain. We explore three issues in particular: (i) the emergence of secondary modulational instabilities of the uniform pattern, leading eventually to localised states, as the domain size $L$ is increased from zero, (ii) the evolution and persistence of the bifurcation structure at large $L$ where one would expect many features of the bifurcation diagrams to converge, in some sense, to the characteristic snaking bifurcation diagram obtained in the infinite domain case, and (iii) the effects of different boundary conditions on the bifurcation structure. In common with previous authors [34, 11] we study the model cubic-quintic Swift–Hohenberg equation

$$w_t = [r - (1 + \partial_{xx}^2)^2]w + sw^3 - w^5, \tag{1.1}$$

where $\partial_{xx}^2 \equiv \partial^2/\partial x^2$. The choice of the cubic-quintic nonlinearity reduces the dependence of pattern wavelength on pattern amplitude that is more pronounced when a 'quadratic–cubic' nonlinearity is taken. We study (1.1) with periodic boundary conditions (PBC), Dirichlet boundary conditions (DBC) given by $w = w_{xx} = 0$ at $x = 0, L$, or Neumann boundary conditions (NBC) given by $w_x = w_{xxx} = 0$ at $x = 0, L$. Figure 1.1 indicates a typical bifurcation diagram for (1.1) in the $(r, ||w||_{L^2})$ plane, using PBC and a domain of size $L = 10\pi$, obtained by numerical continuation. In figure 1.1 and subsequent figures we use the $L^2$-norm defined by

$$N_2 := \left( \frac{1}{L} \int_0^L w(x,t)^2 \, dx \right)^{1/2}, \tag{1.2}$$

as a measure of the solution amplitude. Figure 1.1 shows the intertwining of the two curves of symmetric localised states and the existence of cross-links of asymmetric localised states.

Our main results are, firstly, that with PBC there exists a minimum domain size $L_c \approx 8\pi\sqrt{10}/(3s)$ for the appearance of any secondary modulational instability that would lead to the formation of snaking curves. This result is exact in the limit of small $s$ but appears to be highly accurate even for order-unity values. We note that $L_c$ varies inversely with the subcriticality parameter $s$ in (1.1). Secondly, we discuss the behaviour at the 'top end' of the snake where, due to the finite domain size, the snaking branches connect back to the uniform periodic pattern. Modulated states near this end of the snake have, naturally, been referred to as 'localised holes' [23]. As the domain size $L$ increases, a mode interaction between periodic patterns of adjacent discrete wavenumbers explains how new 'turns' are added to the snake as $L$ increases. Thirdly, we comment on the relation between these results, obtained for PBC, and the bifurcation structure in the cases of DBC and NBC.

The paper is divided into the following sections. In section 2 we apply standard multiple-scales asymptotics to develop the appropriate amplitude equation near $r = 0$ in the limit of small subcriticality $s$. From the resulting Ginzburg–Landau equation we deduce the modulational instabilities that lead to localised states in a finite domain.

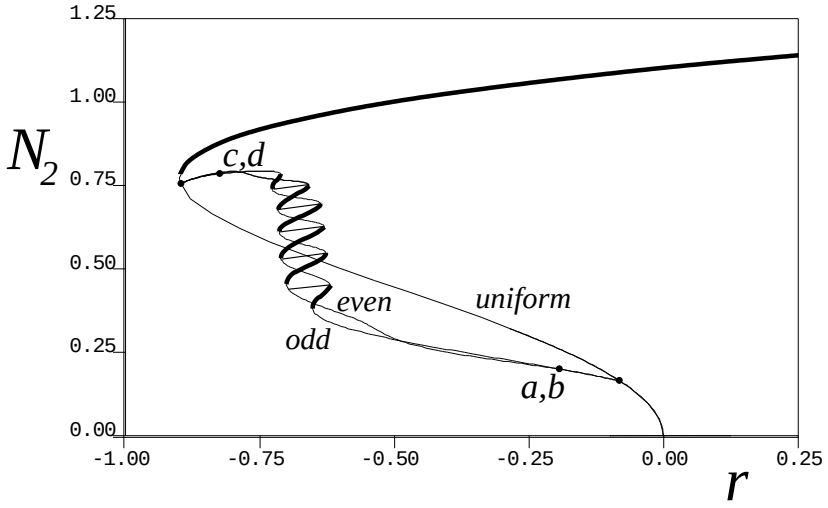


FIG. 1.1. *Bifurcation diagram for (1.1) for $s = 2.0$, in a finite domain $0 \le x \le L = 10\pi$ with PBC, obtained using AUTO07p. Thick and thin lines denote stable and unstable branches respectively. Dots labelled 'a, b' and 'c, d' label the points at which the solutions are as shown in figure 1.2. 'Even' and 'odd' refer to the symmetry of states on the two modulated branches. 'Uniform' denotes the spatially $2\pi$-periodic branch.*

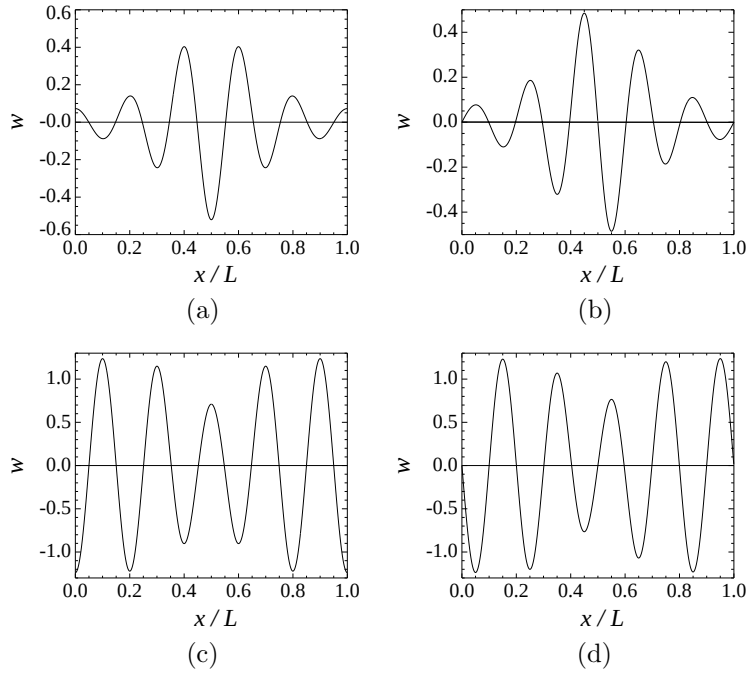


FIG. 1.2. *Numerical solutions to (1.1) on the odd and even branches of modulated solutions. (a) $r = -0.18$, even branch, lower end; (b) $r = -0.18$, odd branch, lower end; (c) $r = -0.83$, even branch, upper end; (d) $r = -0.83$, odd branch, upper end. Parameters: $s = 2.0$, $L = 10\pi$.*

We show that modulational instabilities occur, for fixed $s$, only if the domain is large enough. In section 3 we discuss these instabilities from a symmetric bifurcation theory viewpoint and indicate why exactly two 'snaking' branches appear. In section 4 we return to (1.1) and examine the development of the modulational instability and the persistence of the snaking bifurcation behaviour in a finite domain as $L$ increases. Section 5 discusses the influence of Dirichlet or Neumann boundary conditions, and section 6 concludes.

**2. Ginzburg–Landau theory.** In this section we discuss the implications of the standard multiple-scales analysis of the Swift–Hohenberg equation (1.1) for the dynamics in a large but finite domain $0 \le x \le L$. The usual analysis begins with the examination of the linear stability of the solution $w(x,t) \equiv 0$ to (1.1). Linearising (1.1) and setting $w = \mathrm{e}^{\sigma t + \mathrm{i}kx}$ results in the dispersion relation $\sigma = r - (1-k^2)^2$ and hence an instability occurs when $r = (1-k_j^2)^2$ where $k_j = 2\pi j/L$, for integers $j \ge 1$. In a finite domain of fixed length $L = 2\pi n \gg 1$ we expect solutions near the linear instability threshold $r = 0$ to be of the form

$$w = \varepsilon w_1 + \varepsilon^2 w_2 + \cdots = \varepsilon A(X,T)\mathrm{e}^{\mathrm{i}x} + c.c. + \cdots, \tag{2.1}$$

since the instability at $r = 0$ is to a perturbation with wavenumber exactly unity. We consider the case where the instability is mildly subcritical, i.e. we scale $s = \varepsilon^2 \hat{s}$ and $r = \varepsilon^4 \mu$, and introduce the long length- and time-scales $X = \varepsilon^2 x$ and $T = \varepsilon^4 t$. These differ from the standard Ginzburg–Landau scalings due to the scaling of $s$ which enables the cubic and quintic nonlinearities to be balanced to appear at the same order in the multiple-scales expansion.

Expanding as usual we employ the linear operator $\mathcal{L} \equiv (1 + \partial_{xx}^2)^2$ to obtain a solvability condition at each order. This solvability condition is satisfied by the solution for $w_1(x,X,T)$ noted in (2.1). At $O(\varepsilon^2)$, $O(\varepsilon^3)$ and $O(\varepsilon^4)$ the solvability condition is trivially satisfied. At $O(\varepsilon^5)$ we deduce, from the usual requirement that no secular terms arise in the solution, an evolution equation for the slowly-varying amplitude $A(X,T)$:

$$A_T = \mu A + 4A_{XX} + 3\hat{s}A|A|^2 - 10A|A|^4. \tag{2.2}$$

This equation has nontrivial uniform solutions which satisfy

$$10A_0^4 - 3\hat{s}A_0^2 - \mu = 0. \tag{2.3}$$

There is a saddle-node bifurcation at $\mu \equiv \mu_{sn} = -9\hat{s}^2/40$; the larger-amplitude solution $A_0^+$ exists for all $\mu > \mu_{sn}$ and is stable. Perturbing the uniform solutions and looking for a linear instability we write $A(X,T) = A_0 + a_0\mathrm{e}^{\mathrm{i}\ell X}$, where $\ell = 2\pi m/(\varepsilon^2 L)$ since the finite domain discretises the allowed perturbation wavenumbers. We find that instability occurs when

$$\frac{3\hat{s}}{2}A_0^2 + \mu + \ell^2 = 0. \tag{2.4}$$

Viewing (2.3) and (2.4) in the $(\mu, A_0^2)$ plane (see figure 2.1) and treating $\ell^2$ as a parameter we see that modulational instability first appears as $\ell^2$ is decreased (i.e. the domain expands), when $m = 1$ (i.e. the longest wavelengths are destabilised first) and when $A_0^2 = 3\hat{s}/40$. This corresponds to $\mu = -27\hat{s}^2/160$. Interestingly, this is the same value as the 'Maxwell point' $\mu_{mx}$ obtained by equating the values of

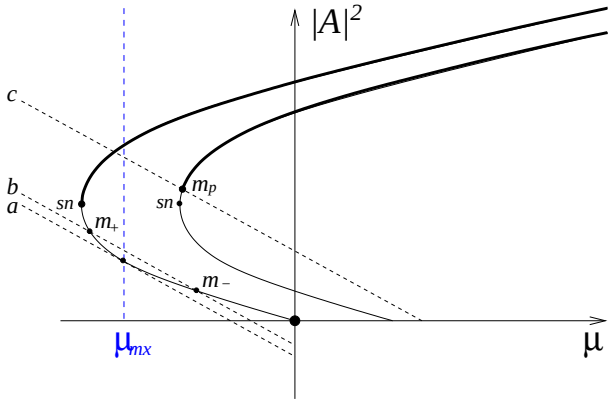


FIG. 2.1. *Sketch bifurcation diagram for the Ginzburg–Landau equation (2.2) indicating the onset of modulational instability. Line a illustrates the marginal case when the uniform state $A = A_0$ becomes unstable in a domain of size $L = L_c \equiv 8\pi\sqrt{10}/(3s)$. Line b indicates that for $L > L_c$ we anticipate that there are two bifurcation points $m_\pm$ where modulational instability occurs. Line b intersects the vertical axis at $A_0^2 = -2\ell^2/(3\hat{s})$. Line c (which intersects the vertical axis at $A_0^2 = 2(5q^2 - \ell^2)/(3\hat{s})$) indicates that the solution $A = R_0 e^{iqX}$ becomes unstable at $m_p$, sketched here as lying above the saddle-node point.*

the first integral of (2.2), setting $\partial_T \equiv 0$, obtained on the trivial $A \equiv 0$ and stable nontrivial $A = A_0^+$ branches. Further algebraic simplification shows that the onset of modulational instability occurs at $\ell^2 = 9\hat{s}^2/160$ which implies (at leading order in $s$) a minimum domain size $L_c = 8\pi\sqrt{10}/(3s)$. This result is illustrated in figure 2.1 where line $a$ corresponds to the critical case $L = L_c$ and line $b$ to $L > L_c$.

Long-wavelength modulational instabilities of this kind are reminiscent of the Eckhaus instability; indeed the modulational instability identified here is exactly that discussed by Tuckerman & Barkley [36] in a finite domain. The correspondance between the calculations is described in detail for the quadratic-cubic Swift–Hohenberg equation by Bergeon et al. [6].

Returning to the Ginzburg–Landau equation (2.2), we examine the existence and stability of solutions of the form $A = R_0 e^{iqX}$, corresponding to periodic patterns with wavenumbers different from, but as near as possible to, unity. More precisely, when $L = 2\pi n \gg 1$, such a solution is $L$-periodic when $\varepsilon^2 q = 1/n \ll 1$. These solutions therefore exist when $10R_0^4 - 3sR_0^2 - (\mu - 4q^2) = 0$, corresponding to the right-hand parabola in figure 2.1. A similar linearised stability calculation to that presented above shows that these solutions undergo a modulational instability when

$$\frac{3\hat{s}}{2}A_0^2 + (\mu - 4q^2) + \ell^2 - q^2 = 0, \tag{2.5}$$

which corresponds to line $c$ in figure 2.1, i.e. a line shifted to the right by the same distance as the parabola, but also shifted upwards by $q^2$ and therefore intersecting the parabola at the point $m_p$, above the saddle-node point $sn$ (for large enough $q^2$).

Figure 2.2 shows the results of numerical investigation of the Ginzburg–Landau equation (2.2). A direct comparison is possible between figure 2.2 and figure 1.1 since $\varepsilon^2 = s/\hat{s} = 1$. Thus the domain size and horizontal axes are rescaled equally. A minor difference is the vertical axis; due to the ansatz 2.1 we have that $||w(x,t)||_{L^2} = \sqrt{2}||A(X,T)||_{L^2}$. Clearly the Ginzburg–Landau equation provides a good asymptotic guide to figure 1.1. Quantitatively, note that the points $\mu_{m+} = -0.8980441$ and

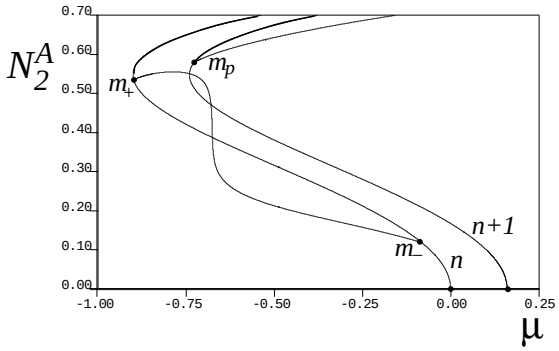


FIG. 2.2. *Numerically computed bifurcation diagram for the Ginzburg–Landau equation (2.2). $\hat{s} = 2$, domain size $\varepsilon^2 L = 10\pi$, i.e. $0 \le X \le 10\pi$. The vertical axis corresponds to the $L^2$-norm $N_2$ defined as in (1.2) but by integrating $|A|^2$ rather than $w(x,t)^2$. Thick and thin lines indicate stable and unstable branches respectively. $n$ and $n+1$ denote branches of spatially-periodic solutions $A = A_0$ and $A = R_0 \mathrm{e}^{\mathrm{i}qX}$, respectively, with $q = 2\pi/(\varepsilon^2 L) = 0.2$. Branches of modulated states bifurcate from these branches at $m_\pm$ and $m_p$.*

$\mu_{m-} = -0.0819559$ in figure 2.2 correspond, respectively, to $r = -0.8971424$ and $r = -0.0794274$ in figure 1.1. Thus the differences are 2.5% or less even when $\varepsilon = 1$. Similarly the saddle-node bifurcation point on the branch of subcritical spatially-periodic states in figure 1.1 occurs at $r = -0.8990114$ which differs by around 0.1% from the estimated value $\mu_{sn} = -9/10$ in figure 2.2.

In large domains where we focus on the case $\ell \ll 1$, the modulational instabilities $m_-$ and $m_+$ occur at distances of $O(\ell^2)$ from $\mu = 0$ and from the saddle-node bifurcation point $\mu = \mu_{sn}$, respectively. Numerical investigation shows that a branch of modulated states connects $m_+$ to $m_-$. These modulated states develop an angular shape; the $L^2$-norm remains small as $\mu$ first decreases from $m_-$ (and $A(X)$ has a peaked, *sech*-like, profile) until $\mu \approx \mu_{mx}$ at which point the $L^2$-norm increases rapidly (and $A(X)$ resembles a pair of *tanh*-like fronts). As $\mu$ is decreased further, towards $m_+$, the solution resembles a uniform amplitude state with a localised 'hole' where the pattern amplitude is slightly reduced. The modulated branch bifurcating from $m_p$ similarly corresponds to a 'hole' in the amplitude of a modulated pattern. The proximity of these two branches of modulated states indicates the possibility that these secondary branches arise through mode interactions between spatially-periodic branches of nearly equal wavenumbers. We return to this point in section 4.

**3. Symmetric Bifurcation Theory.** In this section we discuss the constraints placed by symmetry on the bifurcations of (1.1) in a finite domain with PBC. In this case the relevant symmetry group is $O(2) \times \mathbb{Z}_2$. At $r = 0$ we suppose that there is a linear instability of $w(x,t) \equiv 0$ to an eigenfunction $w(x,t) = z(t)\mathrm{e}^{\mathrm{i}kx} + c.c.$ and periodicity implies $L = 2\pi n/k$ so that $n$ spatial periods fit into the domain. The symmetry group $O(2) \times \mathbb{Z}_2$ is generated by translations and reflections:

$$\begin{aligned} &\tau_\delta : x \to x + \delta;\ z \to z\mathrm{e}^{\mathrm{i}k\delta}, \\ &m : x \to L - x;\ z \to \bar{z}, \\ &\kappa : w \to -w; \qquad z \to -z. \end{aligned}$$

Immediately we see that all solutions have symmetry $\kappa\tau_\pi$, i.e. a half-period translation followed by a change of sign. The equivariant amplitude equation takes the form

$\dot{z} = \mu z + az|z|^2 + \cdots$, i.e. of the same form as the Ginzburg–Landau equation (2.2) but omitting the $X$-derivative terms. Due to translational symmetry the phase of $z$ is undetermined, and a circle of bifurcating modes exists (often referred to as a 'pitchfork of revolution'). Two fixed-point subspaces are of particular interest: Fix($m$) and Fix($m\kappa$). Solutions within Fix($m$) obey NBC since if $w(x,t) = w(L-x,t) = w(-x,t)$ using $L$-periodicity then, differentiating $j$ times with respect to $x$ and setting $x = 0$, we obtain $w^{(j)}(0,t) = (-1)^j w^{(j)}(L,t) = (-1)^j w^{(j)}(0,t)$ and so odd derivatives of $w(x)$ vanish at $x = 0, L$. Similarly, within Fix($m\kappa$) we have $w(x,t) = -w(L - x,t) = -w(-x,t)$ and so $w^{(j)}(0,t) = (-1)^{j+1} w^{(j)}(L,t) = (-1)^{j+1} w^{(j)}(0,t)$ which implies that even derivatives of $w(x)$ vanish at $x = 0, L$ and $w(x,t)$ obeys DBC. Since Fix($m\kappa$) = Fix($m\tau_\pi$) it is clear that when PBC are used, all these spatially-periodic states are related by translation symmetries. Therefore, with PBC, they lie on a single group orbit and have identical stability properties.

Returning to PBC, now let us consider a (fully nonlinear) spatially-periodic state $w_p(x) = w_p(x + \frac{L}{n})$. Without loss of generality we select a state lying in Fix($m$). Looking for a modulational instability on the scale of the domain we look at the action of the symmetries in the isotropy subgroup of $w_p(x)$ on the amplitude $v(t)$, where $w(x,t) = w_p(x) + v(t)\mathrm{e}^{\mathrm{i}kx/n} + \bar{v}\mathrm{e}^{-\mathrm{i}kx/n}$:

$$\kappa\tau_\pi : v \longrightarrow -v\mathrm{e}^{\mathrm{i}k\pi/n}, \qquad m : v \to \bar{v}. \tag{3.1}$$

Clearly $(\kappa\tau_\pi)^2 = \tau_{2\pi}$ is an element of order $n$, so that $\kappa\tau_\pi$ has order $2n$ and does not commute with $m$ (in fact $\kappa\tau_\pi m\kappa\tau_\pi = m$) so that together $\kappa\tau_\pi$ and $m$ generate the group $D_{2n}$, the symmetry group of rotations and reflections of a planar regular $2n$-gon.

The general description of bifurcations with $D_{2n}$ symmetry is well known, see for example [18]. In the discussion below, and for the remainder of the paper, we assume $n \geq 2$ and discuss the 2D irreducible representation of $D_{2n}$ generated by (3.1) (the case $n = 1$ is special since $D_2 \simeq \mathbb{Z}_2 \times \mathbb{Z}_2$ has only 1D irreducible representations). For $n \geq 2$ there are two distinct axial isotropy subgroups: $\mathbb{Z}_2[\kappa\tau_\pi m]$ and $\mathbb{Z}_2[m]$. Hence, by the Equivariant Branching Lemma, solution branches with these isotropy subgroups are guaranteed to exist. In fact it can be shown that, generically, there are no other bifurcating equilibria. Geometrically the two branches correspond to the preservation of a single reflection symmetry of the planar $2n$-gon; the axis of the reflection either passes through a pair of opposite corners or through the midpoints of a pair of opposite sides. The stability properties of these two branches will typically differ, although for $n \geq 4$ consideration of the amplitude equations indicates that the bifurcations are pitchforks within each fixed-point subspace, and that the branches generically bifurcate in the same direction. In the situation at hand the $\mathbb{Z}_2[\kappa\tau_\pi m]$-symmetric branch corresponds to a modulated state that is odd-symmetric about $x = (L - \pi)/2$ and the $\mathbb{Z}_2[m]$-symmetric state corresponds to a state that is even-symmetric about $x = L/2$.

Restricting the above discussion to NBC, discarding the translational symmetry $\tau$, we conclude that an initial state $w_p(x) \in$ Fix($m$) undergoes a pitchfork bifurcation (due, from this viewpoint, to a 'hidden symmetry') that preserves the reflection symmetry $m$ and so leads to (a single snaking curve of) even-symmetric modulated states. Similarly, an initially $2\pi$-periodic state $w_p(x) \in$ Fix($\kappa m$) leads to a $D_{2n}$-symmetric bifurcation with axial branches with symmetry $\mathbb{Z}_2[m\tau_\pi]$ and $\mathbb{Z}_2[\kappa m]$. Solutions on the $\mathbb{Z}_2[m\tau_\pi]$ branch are even-symmetric about the point $x = (L - \pi)/2$ and those on the $\mathbb{Z}_2[\kappa m]$ branch are odd-symmetric about the midpoint $x = L/2$. Likewise,

when DBC are imposed, the $\mathbb{Z}_2[\kappa m]$ branch persists and leads to a snaking curve of odd-symmetric states.

**4. Snaking behaviour.** In this section we examine how the Ginzburg–Landau theory and the predictions from symmetric bifurcation theory of the previous sections relate to numerical continuation of solutions to (1.1).

The bifurcation and continuation software AUTO07p [17] was used to solve (1.1) as a boundary value problem on a finite domain. The primary branches of spatially periodic solutions were computed by imposing either DBC ($w = w_{xx} = 0$ at $x = 0, L$), or NBC ($w_x = w_{xxx} = 0$ at $x = 0, L$); both of these remove the continuous translational symmetry that would otherwise cause numerical difficulty. As we have seen, each of DBC and NBC undergoes a secondary bifurcation to produce exactly one of the two spatially-modulated branches we expect to identify during numerical continuation along these branches. Numerical continuation using PBC can be achieved if, in addition to imposing the periodicity of $w$ and its first and second derivatives, a constraint to fix the 'phase' (i.e. the origin in $x$) of the solution is used. To do this we implement the integral phase constraint in the form proposed by Rademacher et al [30]; this is found to provide excellent numerical stability. Specifically, the integral condition

$$\int_0^1 \langle U'(x), U_{\rm old}(x) - U(x)\rangle = 0 \tag{4.1}$$

is implemented in the AUTO subroutine ICND via the code

```
FI(1)=0.0
do j=1, NDIM
FI(1) = FI(1) + UPOLD(j) * (UOLD(j) - U(j))
end do
```

where the fourth-order ODE is rewritten as the first-order system $U_x = F(U)$ for the vector $U = (w, w_x, w_{xx}, w_{xxx})$, and $U_{\rm old}(x)$ is the solution to the boundary-value problem at the previous continuation step.

The discussion of the evolution of the snaking diagram as $L$ increases is divided between the following two subsections: in section 4.1 we note that the bifurcation diagram changes rapidly at domain sizes $L$ which are close to those for which there is a codimension-two linear instability of the trivial branch $W(x,t) \equiv 0$, and describe the codimension-two bifurcation involving a pair of fully nonlinear spatially-periodic states. In section 4.2 we turn our attention to the detailed evolution of the branches of modulated states.

**4.1. Mode interactions and bifurcations to modulated branches.** It is straightforward to describe the mode interaction that occurs in the linear instability of the trivial solution $w(x,t) \equiv 0$. The trivial solution is simultaneously linearly unstable to periodic patterns that fit $n$ and $n+1$ pattern wavelengths into the domain of size $L$ when $1 - (2\pi n/L)^2 = (2\pi(n+1)/L)^2 - 1$, i.e. at $L = \pi\sqrt{4n^2+4n+2}$. For the cases $n = 2, 3, 4$ this yields the values $L = 16.019, 22.214, 28.448$ to 3 d.p. respectively; these values are indicated by the horizontal dashed lines in figure 4.3.

The fully nonlinear spatially-periodic pattern branches also collide at codimension-two points where the curves in the $(r, L)$ plane on which they undergo saddle-node bifurcations coincide. Figure 4.2 shows the numerically-determined location of these

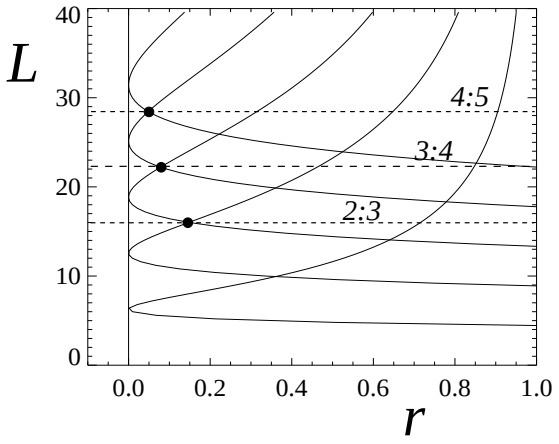


FIG. 4.1. *Linear stability curves* $r = [1 - (2\pi j/L)^2]^2$ *for* $1 \le j \le 5$ *in the* $(r, L)$ *plane for (1.1) using PBC. Dots indicate the codimension-two points at which there are mode interactions in the linear instability of the trivial state* $w(x,t) \equiv 0$. *The corresponding values of* $L$ *are indicated by the horizontal lines which are reproduced on figure 4.3.*

saddle-node bifurcations for the case $n = 4$ (i.e. the patterns with period $L/4$ and $L/5$). The codimension-two point is labelled $M$.

Separately, the bifurcation points $m_+$ and $m_p$ move up and down the spatially-periodic branches. To within the numerical precision used, it appears that they cross through the saddle-node points at the same value of $L$; this is due to the very weak dependence of the pattern wavelength on amplitude.

The behaviour of the bifurcation points $m_+$ and $m_p$ can be understood through a straightforward consideration of the relevant amplitude equations near the codimension-two point $M$ in the $(r, L)$ parameter plane where the saddle-node bifurcations of the fully-nonlinear periodic patterns coincide. We combine the requirements that *(i)* the periodic fully nonlinear patterns with amplitudes $a(t)w_n(x)$ and $b(t)w_{n+1}(x)$ lie in different fixed-point subspaces, and *(ii)* they undergo nearby saddle-node bifurcations, generically at slightly different amplitudes. We also take only the leading-order couplings between the modes. These considerations result, after rescaling, in amplitude equations of the form

$$\dot{a} = a\left[\lambda - (a-1)^2 + \alpha b\right], \tag{4.2}$$

$$\dot{b} = b\left[\mu - (b-\gamma)^2 + \beta a\right], \tag{4.3}$$

where we anticipate that $\gamma \approx 1$. Clearly there are periodic pattern solutions $\{a_\pm = 1 \pm \sqrt{\lambda}, b = 0\}$ and $\{a = 0, b_\pm = \gamma \pm \sqrt{\mu}\}$ which exist only when $\lambda > 0$ and $\mu > 0$ respectively. The equilibria $(a_\pm, 0)$ undergo bifurcations to mixed-mode equilibria (i.e. $ab \neq 0$) when $\mu + \beta - \gamma^2 \pm \beta\sqrt{\lambda} = 0$, respectively. The curves on which a mixed-mode bifurcates from $(a_\pm, 0)$ are labelled $m_p^n$, $m_+^n$, respectively, in figure 4.2(b). Similarly, the equilibria $(0, b_\pm)$ undergo mixed-mode instabilities when $\lambda - 1 + \alpha\gamma \pm \alpha\sqrt{\mu} = 0$. These instabilities are labelled $m_p^{n+1}$ and $m_+^{n+1}$, respectively, in figure 4.2(b). Overall, the sketch bifurcation diagram in figure 4.2(b) confirms, qualitatively, the numerical results shown in figure 4.2(a).

We remark also that the values of $L$ that correspond to the codimension-two

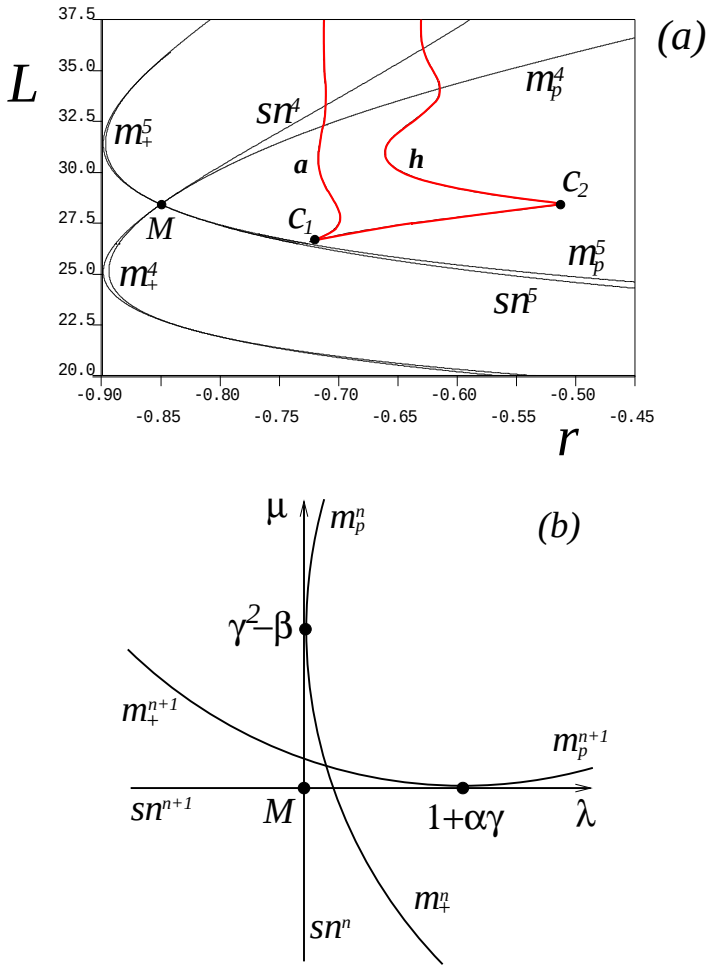


FIG. 4.2. *(a) Numerically determined location, in the $(r, L)$ plane, of saddle-node bifurcations $sn^4$ and $sn^5$ for periodic patterns with periods $L/4$ and $L/5$, respectively, and the corresponding modulational instabilities $m_+^4$ and $m_+^5$. The curve of saddle-node bifurcations, labelled a and h, passing through the points $c_1$ and $c_2$ bounds the region within which new stable modulated or localised states appear. These curves are also shown on figure 4.3. (b) Sketch bifurcation diagram near the codimension-two point M (when $n = 4$) for the amplitude equations (4.2) - (4.3).*

bifurcations of the fully nonlinear periodic branches, for example $M$ in figure 4.2, are extremely close to those given by the mode interactions in the linear instability of $w(x,t) \equiv 0$. This is, again, due to the very small variation in wavenumber of the periodic solutions as they evolve to large amplitude.

**4.2. Reattachment of the snaking branch.** Having discussed the spatially-periodic branches, and the bifurcation points at which the modulated states appear, we now turn to the sequence of bifurcations through which the snaking branch is transferred over from one periodic branch to the next, as $L$ increases. This sequence of transitions occurs over an extremely small region of parameter space, and away from both the spatially-periodic branches.

We first observe that a snaking branch develops a pair of additional saddle-node

bifurcations as $L$ increases; the top end of the snake distorts as this new twist in the snake grows. The extent of this twist is shown in figure 4.3 which shows the regions of existence of the localised states on each 'level' of the finite snake shown in figure 1.1. Since the two snaking branches (even-symmetric and odd-symmetric) lie in different fixed point subspaces the details of the evolution of these branches need not be identical, and as figure 4.3 shows, the location of the cusp point (e.g. $c_1$) at which the saddle-nodes appear is different in the two cases. Figure 4.3 shows that localised

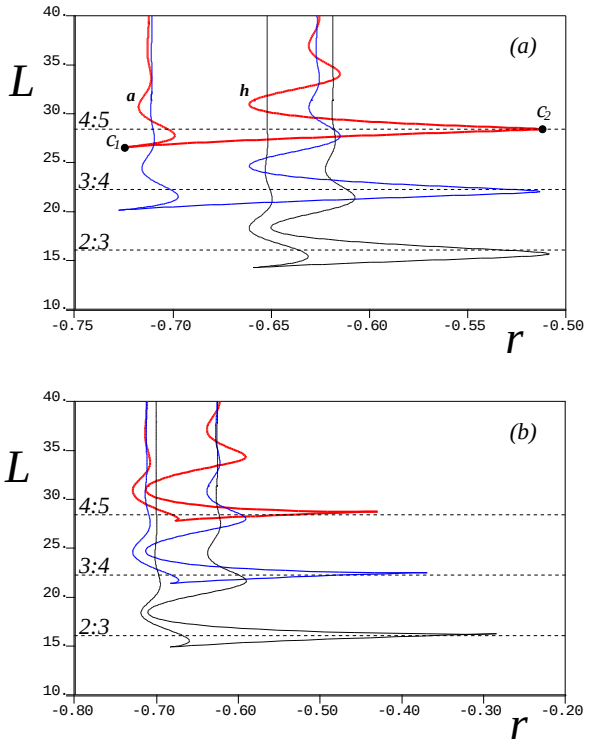


FIG. 4.3. *Saddle-node bifurcation curves of (1.1) using PBC. These curves form the boundaries of the regions of existence, in the $(r, L)$ plane, of localised states with increasing numbers of bumps: (a) Odd-symmetric states (b) Even-symmetric states. Pairs of saddle-node bifurcations appear at the cusps as $L$ increases. The points $c_1$ and $c_2$ correspond to those indicated in figure 4.2(a). The curves of saddle-node bifurcations that extend from $c_1$ are labelled $a$ and $h$ and appear also in figures 4.7, 4.4 and 4.5. Dashed lines indicate the values of $L$ at which $n : n+1$ mode interactions occur in the linear instability of $w = 0$, see figure 4.1.*

states on the 'lower levels' of the snake settle quickly to occupy a region in $r$ either side of the Maxwell point $r = r_{mx} \approx -0.675$, bounded by saddle-node bifurcations that remain at fixed locations in $r$ as $L$ increases. New 'twists' on the snake are born regularly as $L$ increases by $2\pi$; a pair of saddle-node bifurcations appears near the top of the snake at $r \approx -0.73$ (for odd-symmetric states) or $r \approx -0.68$ (for even-symmetric states). As $L$ increases, one of these saddle-node points moves rapidly into $r > r_{mx}$, reaching a maximum value of $r$ at the point $c_2$ which is not, in fact, another cusp, but a smooth maximum as can be seen from figure 4.7.

We now present a detailed discussion of the bifurcation structure surrounding one reattachment event, for the odd-symmetric snaking curve at a domain size $L \approx 28$. At

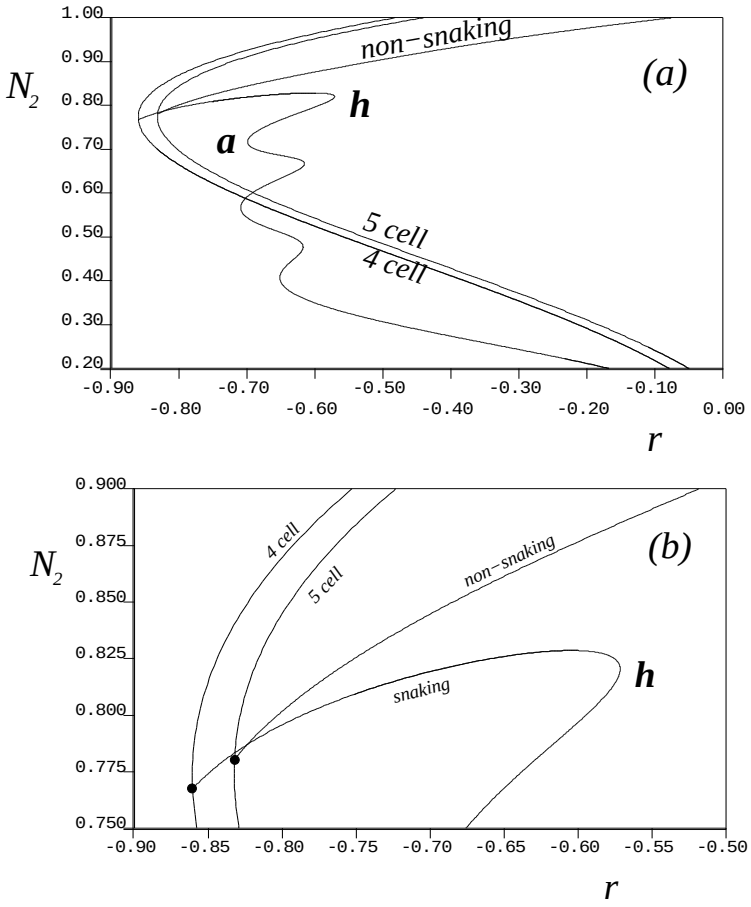


FIG. 4.4. *Numerically-determined bifurcation diagrams in the* $(r, N_2)$ *plane for* $L = 28.0$ *(i.e. below the codimension-two point M in figure 4.2). (a) shows the two branches of spatially-periodic* 4 *and* 5*-cell states which approach each other, together with the two secondary branches of odd-symmetric modulated states which interact as L increases further. (b) is an enlargement of (a) showing that the snaking secondary branch connects to the* 4*-cell periodic branch and the non-snaking branch connects to the* 5*-cell periodic branch. The saddle-node bifurcations a and h are born in the cusp at* $c_1$ *in figure 4.3(a).*

any value of $L$, this detailed discussion involves up to eight saddle-node bifurcations which are labelled $a, \ldots, h$ on the figures in this section. Not all saddle-nodes appear on every figure.

Figure 4.4 corresponds to a bifurcation diagram above the point $c_1$ in figure 4.3(a); the two saddle-node bifurcations $a$ and $h$ at the top of the snaking curve were created in the cusp at $c_1$ as $L$ increased. Figure 4.4(b) shows that for $L = 28.0$ the snaking branch still connects to the 4-cell spatially-periodic branch, and that the 5-cell periodic branch has a secondary bifurcation to a modulated branch which extends monotonically into $r > r_{mx}$.

Although figure 4.4 shows solution branches to the Swift–Hohenberg equation, it is useful to point out the correspondance between the points $m_+$ and $m_p$ in figure 2.2 and the bifurcations to secondary branches indicated by the black dots in figure 4.4(b).

As $L$ increases further, the non-snaking mixed-mode branch that extends to large positive $r$ is found to acquire a number of additional saddle-node bifurcations, before the snaking branch reattaches to the 5-cell branch. This is perhaps unexpected, but corresponds with behaviour found in the quadratic-cubic Swift–Hohenberg case [6], and indeed, for the cubic-quintic case by other authors [9, 10].

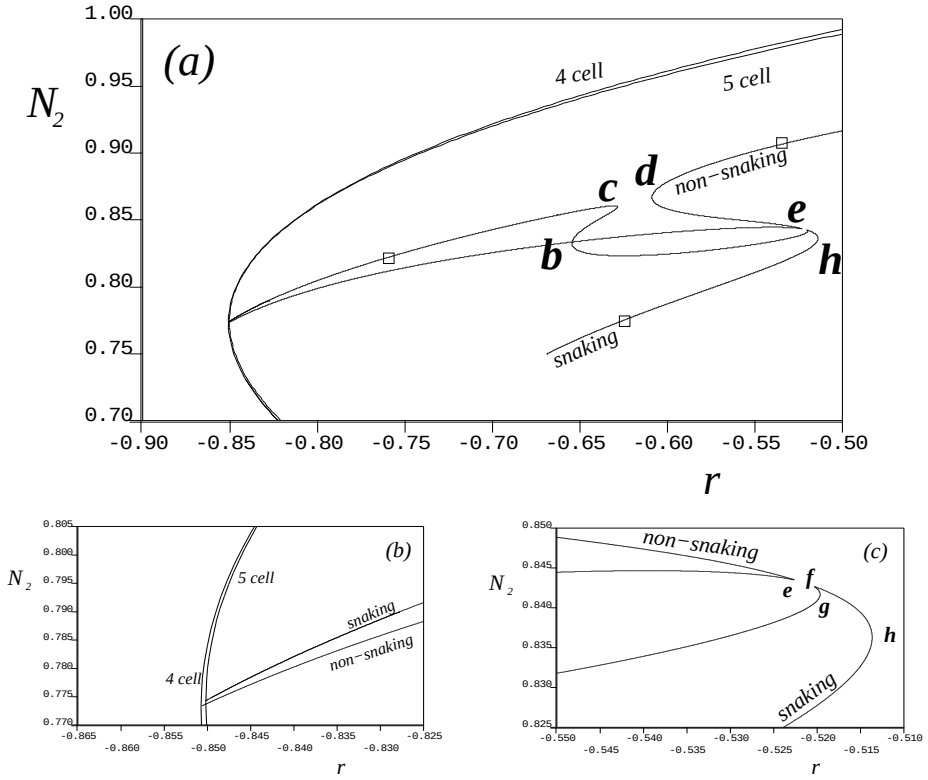


FIG. 4.5. *Numerically-determined bifurcation diagrams in the* $(r, N_2)$ *plane for* $L = 28.4215 > L_{tc}$. *(a) shows the overall arrangement of the two branches of spatially-periodic* 4 *and* 5*-cell states which approach each other, together with the two secondary branches of odd-symmetric modulated states which interact as* $L$ *increases further. Labels b, c, d, e and h indicate saddle-node bifurcations and correspond to the labels in figure 4.7. (b) is an enlargement of (a) showing that the two secondary branches still connect one to each of the* 4*-cell ad* 5*-cell spatially-periodic branches. (c) is an enlargement showing that the branches now 'pinch-off' at* $r \approx -0.522$ *instead of crossing without bifurcation as was the case at smaller* $L$. *Saddle-nodes f and g exist in (a) but are not labelled for practical reasons since they occur very close together.* □ *symbols correspond to solution profiles* $w(x)$ *given in figure 4.6.*

Figure 4.5 shows how the two secondary branches deform as the additional saddle-node bifurcations appear. As one moves up the snaking branch, after the saddle-node $h$ the solutions now encounter two additional saddle-nodes at $f$ and then $g$ before moving to more negative $r$ along what was previously the 'non-snaking' branch and encountering the saddle-node bifurcations at $b$, and finally $c$, before connecting to the 5-cell periodic branch. In contrast, the non-snaking branch that extends to large positive $r$ now (as $r$ is decreased from positive values) undergoes saddle-node bifurcations at $d$ and then $e$, coming close to the snaking branch, before moving to more negative $r$ and connecting to the 4-cell spatially-periodic branch. Note that the

saddle-node at $g$ has switched branches.

The key event, therefore, is the appearance of the saddle-nodes at $e$ and $f$ which cause the secondary branches to 'pinch-off' and reconnect in a new way. This event is a two-parameter unfolding of a standard transcritical bifurcation; we denote the value of $L$ at which it occurs by $L_{tc}$; this is indicated by a dashed line in figure 4.7(a) and (b).

The profile of the solution $w(x)$ changes remarkably little along solution curves as these saddle-node bifurcations appear and disappear. Figure 4.6 shows the solution form at four points indicated by black dots in figure 4.5. Figure 4.6(a) shows a solution coming up from the snaking branch, with a periodic pattern almost filling the domain. In figure 4.6(b), corresponding to point $f$ in figure 4.5(c) this solution develops a central 'almost-flat' region which further evolves, as $r$ decreases, towards the spatially-periodic 5-cell branch in figure 4.6(c). For comparison, figure 4.6(d) shows a solution on the non-snaking branch in which the central 'defect' in the structure will persist at large positive $r$.

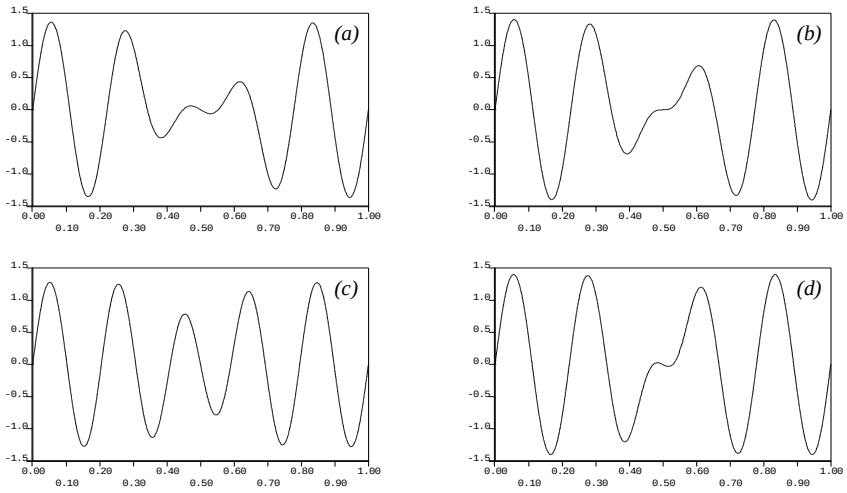


FIG. 4.6. *Solution profiles, plotting $w(x)$ against $x/L$ at four points on figure 4.5. Points (a), (c) and (d) are indicated on figure 4.5(a) by $\square$ symbols. (a) $r = -0.6203$ on the snaking branch. (b) $r = -0.5203$ at saddle-node point $f$. (c) $r = -0.7513$ on the snaking branch before it terminates on the 5-cell periodic branch. (d) $r = -0.5306$ on the non-snaking branch.*

Overall, as $L$ increases the bifurcation structure evolves as successive curves of spatially-periodic patterns appear from large positive $r$, and interact as shown in figure 4.2 with the curve of periodic patterns bifurcating from $w(x,t) \equiv 0$ at the lowest value of $r$. Over a remarkably small region of $L$ this interaction generates saddle-node bifurcations on the secondary branches of spatially-modulated states leading, ultimately, to the reattachment of the snaking curve to the new uniform pattern branch and an extra 'turn' being added to the top of the snaking curve. The spatially-periodic branches then separate as the one with the smaller number of cells moves away to large positive $r$ and the process repeats.

In the case of the Swift–Hohenberg equation with a quadratic-cubic nonlinearity [6] it has been observed that two distinct transitions take place as $L$ increases. These are referred to as type I and type II. In the cubic-quintic problem discussed here it has

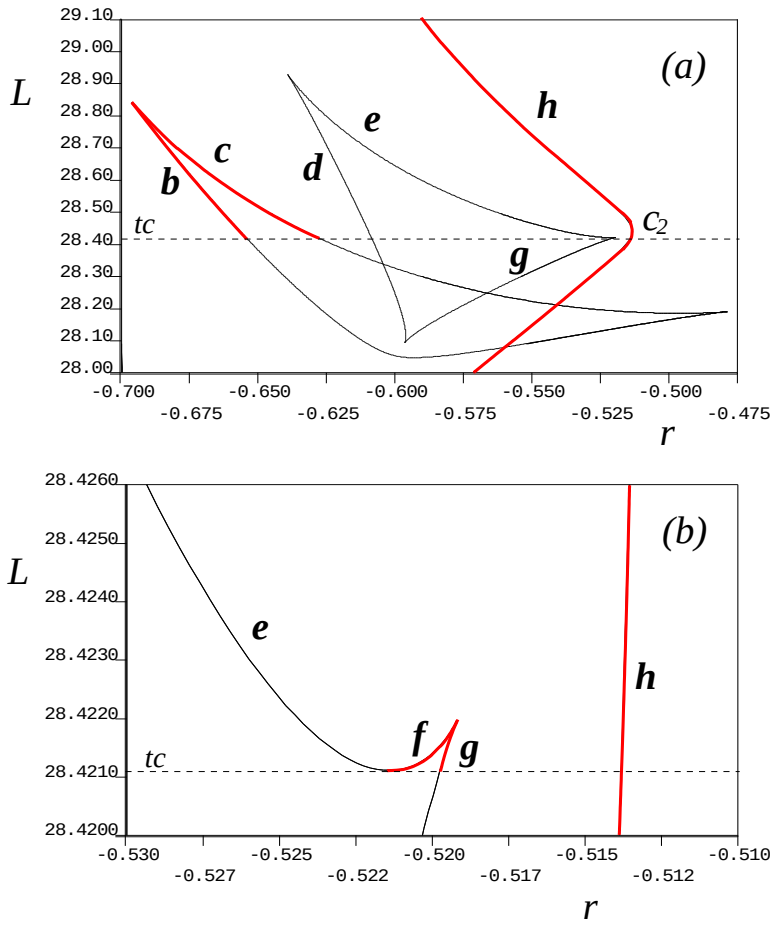


FIG. 4.7. *Numerically-determined location in the $(r, L)$ plane of the additional saddle-node bifurcations that organise the reattachment of the snaking branch as $L$ increases. The transcritical bifurcation occurs at $L = L_{tc}$, $r \approx -0.521$. The dashed horizontal line corresponds to $L = L_{tc}$. Saddle-nodes are indicated by thick red lines if they occur on the snaking branch, and by thin black lines if they occur on the non-snaking branch. As $L$ increases through $L_{tc}$ this distinction causes saddle-nodes b, c and g to shift immediately from one curve to the other; this is indicated by the change inline style, although the position of each saddle-node point varies smoothly. The point $c_2$ corresponds to that indicated in figure 4.2(a). Note that saddle-node a does not appear in (a) or (b): it remains at more negative values of $r$ throughout.*

been found [9, 10] that the observed transitions are all of the same type, corresponding to 'type II' in the terms used by [6].

**5. Dirichlet and Neumann boundary conditions.** In this section we examine the effect of replacing the periodic boundary conditions with Dirichlet or Neumann ones. First, we discuss solutions in a smaller domain ($L = 6\pi$) where the bifurcation structure is simpler and the differences are more pronounced. The bifurcation diagram for (1.1) with DBC is shown in figure 5.1. As discussed in section 3, only a single zero eigenvalue now occurs at the modulational instability at $m_{\pm}$; the bifurcations are pitchforks and two new solution branches exist in $r_{m+} < r < r_{m-}$. The inset figures in figure 5.1(a) show that one branch corresponds to states with larger amplitude in

the centre ('centre-localised'), and the other to states with larger amplitudes near the boundaries ('edge-localised'). Solutions on both branches are symmetric under $\kappa m : w(x) \to -w(L-x)$, but, crucially, solutions on the two branches do not lie on the same group orbit due to the lack of translational symmetry.

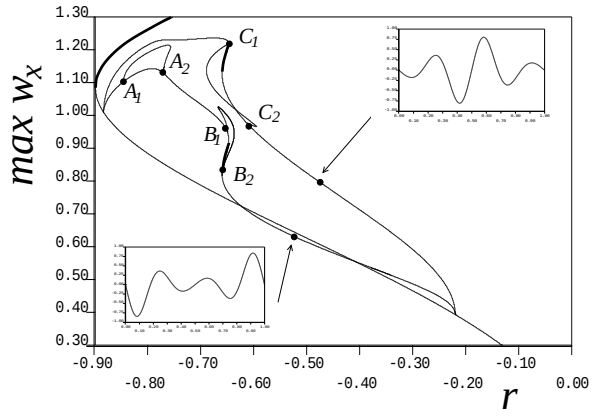


(a)

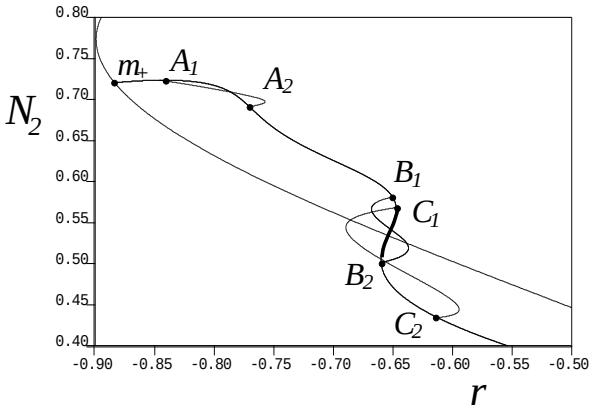


(b)

FIG. 5.1. *Bifurcation diagrams for steady states of (1.1) with DBC in a small domain: $L = 6\pi$, $s = 2.0$. (a) Plot in the $(r, \max(w_x))$ plane with inserts showing modulated states on the two halves of the pitchfork branch, now unrelated by symmetry, at $r = -0.520$ (lower left) and $r = -0.487$ (upper right). Note that each has the symmetry $\kappa m$. Thick and thin lines denote stable and unstable solutions, respectively. (b) An enlargement of (a) plotting the $L^2$-norm on the vertical axis, showing that the branches of modulated states are superimposed.*

As a result, the two branches may (and in fact do) undergo different subsequent bifurcations. Plotting $\max(w_x)$ on the vertical axis clearly distinguishes the two halves of the pitchfork, see figure 5.1(a). It should be noted that plotting the usual $L^2$ norm does not distinguish the branches and this superposition leads to ambiguity in the interpretation of the bifurcation diagram, see figure 5.1(b).

Along the branches of modulated states between $r = r_{m+}$ and $r = r_{m-}$, three further pairs of pitchfork bifurcations occur, labelled $A_1$–$A_2$ and $B_1$–$B_2$ (on the edge-localised branch), and $C_1$–$C_2$ (on the centre-localised branch) in figure 5.1. Each of $A_1$–$A_2$, $B_1$–$B_2$ and $C_1$–$C_2$ produces a closed 'bubble' of asymmetric states. Within

bubbles $B_1$–$B_2$ and $C_1$–$C_2$ each branch undergoes an additional pair of saddle-node bifurcations and so becomes stable over a small interval, as shown by the thick lines in figure 5.1. This interval is slightly different on the two branches since it lies both between the saddle-nodes and between the respective bifurcations to asymmetric states.

We now turn to computations with Neumann boundary conditions; these produce an analogous bifurcation structure, shown in figure 5.2. With NBC, the space-periodic uniform pattern that bifurcates from $r = 0$ is phase-shifted spatially by $\pi/2$ so that it has turning points at $x = 0, L$ and the symmetry $m$. Pitchfork bifurcations (due to 'hidden symmetry') to modulated states occur at exactly the same parameter values as for DBC, and lead to the solution branches shown in figure 5.2 As for DBC, three pairs of pitchfork bifurcations occur subsequently, on the two branches of modulated states which are, again, not on the same group orbit. These pitchfork bifurcations are labelled $D_1$–$D_2$, $E_1$–$E_2$ and $F_1$–$F_2$ in figure 5.2. There is a small interval in $r$ over which the symmetric modulated states are stable. In contrast to the DBC case, in the NBC case the centre-localised state undergoes two pairs of pitchfork bifurcations ($E_1$–$E_2$ and $F_1$–$F_2$) rather than one, and the second of these occurs very close to the lower end of the branch. Both NBC branches also undergo a pair of saddle-node bifurcations, resulting in intervals in $r$ within with the modulated states are stable. These are indicated by thick lines in figure 5.2.

Since the invariant subspaces $\mathrm{Fix}(\kappa m)$ and $\mathrm{Fix}(m)$ contain the two primary curves of localised states, superimposing the bifurcation diagrams for DBC and NBC produces intertwined curves that very closely resemble those obtained with PBC. However, the cross-link branches do not appear in such a superposition. The specification of either DBC or NBC constrains the 'asymmetric' states that bifurcate in the 'bubbles' referred to above so that it is not possible to continuously deform an odd-symmetric state (satisfying DBC) into an even-symmetric one (satisfying NBC). Instead of a cross-link, we find that two neighbouring 'bubbles' approach each other and then separate again, returning to the same curve that they bifurcated from, see figure 5.3 for which the domain size is increased to $L = 10\pi$.

Figure 5.3 shows that the even–symmetric state at $a$ (corresponding to the blue localised state in the inset in figure 5.3b) undergoes a pitchfork bifurcation to produce an asymmetric branch bifurcating to the right. This asymmetric branch then turns around at a saddle-node bifurcation at $b$ (corresponding to the black curve in figure 5.3b) and it then returns to the vicinity of the original even-symmetric solution branch (with another saddle-node point at $c$ (red curve in figure 5.3b)). At $c$ the solution is nearly reflection-symmetric, but with the reflection symmetry not through the midpoint of the domain. The asymmetric branch extends below $c$, remaining very close to the symmetric branch, and terminating at another pitchfork bifurcation on the symmetric branch at larger $r$; this final bifurcation point is not shown, but the overall behaviour is qualitatively as shown in figure 5.2 for the $F_1$–$F_2$ bubble. Between $H_1$–$H_2$ there is a similar branch of asymmetric states which bifurcates from the odd-symmetric snaking curve. It, too, is frustrated by the (in this case Dirichlet) boundary condition and approaches half-way towards the even-symmetric curve before returning to the odd-symmetric branch. This behaviour is similar to the $C_1$–$C_2$ bubble shown in figure 5.1, and is consistent with the mathematical analysis of Beck et al. [4].

**6. Summary.** In this paper we have investigated the bifurcation behaviour of a model PDE (the Swift–Hohenberg equation with cubic and quintic nonlinearities) that undergoes a subcritical Turing-type pattern-forming instability constrained in a

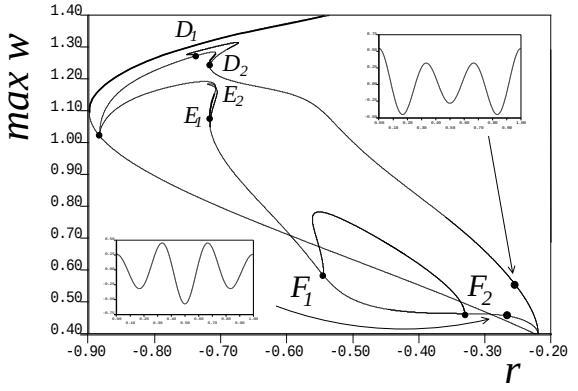


(a)

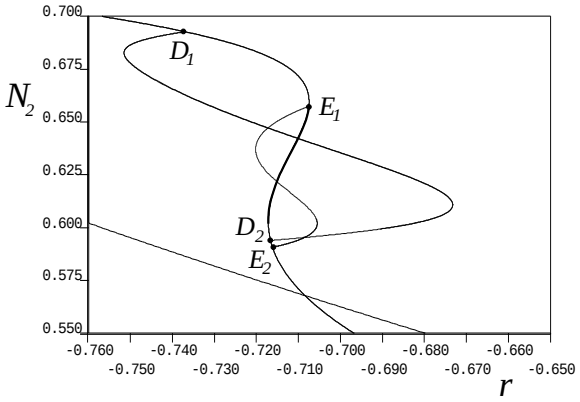


(b)

FIG. 5.2. *Bifurcation diagrams for steady states of (1.1) with NBC in a small domain:* $L = 6\pi$, $s = 2.0$. *(a) Plot in the* $(r, \max(w)$ *plane with inserts showing modulated states on the two halves of the pitchfork branch, now unrelated by symmetry, at* $r = -0.26$ *(lower left) and* $r = -0.25$ *(upper right). Note that each has the symmetry* $m$. *Thick and thin lines denote stable and unstable solutions, respectively. (b) An enlargement of (a), plotting the* $L^2$*-norm on the vertical axis, showing that the even-symmetric branches are superimposed.*

finite domain. Understanding the effects of a finite domain is clearly of interest when comparing experimental and numerical results with theoretical predictions. The finite domain (and the use of Dirichlet or Neumann boundary conditions) modifies the existence of localised states that have been investigated in detail for the 'perfect' infinite domain case [11, 24]. The multiple-scales analysis in section 2 indicates that there is a minimum domain size necessary for the formation of localised states, and, in small domains, these states are only moderately 'localised'; they more closely resemble amplitude-modulated versions of the periodic patterns that they bifurcate from. They are stabilised after further pitchfork and saddle-node bifurcations along the 'snaking' branches, and are stable, in small domains, over a much smaller interval in the bifurcation parameter $r$ than predicted by the width of the snake in the formally infinite-domain case.

As the domain size $L$ increases, successive mode interactions occur which explain how more 'turns' appear on the snaking curves, and how the localised states remain

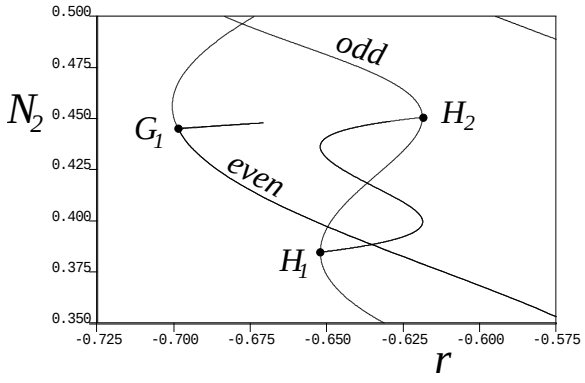


(a)

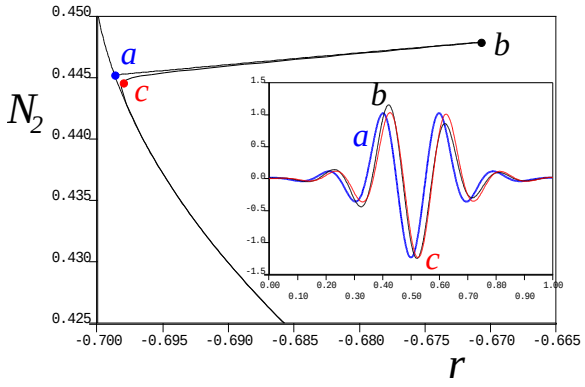


(b)

FIG. 5.3. *Two 'bubbles' of asymmetric states produce a broken 'cross-link', superposing the DBC and NBC bifurcation diagrams for $L = 10\pi$, $s = 2.0$. (a) Even-symmetric branch produces a pitchfork bifurcation at $G_1$; this bubble closes at larger $r$ (not shown); Odd-symmetric branch produces a bubble of asymmetric states between $H_1$–$H_2$. (b) Enlargement of (a) with an inset plot of the localised states at points a, b and c. Point a in (b) is the same as point $G_1$ in (a).*

near the Maxwell point despite the branches of uniform patterns shifting substantially in $r$ as $L$ increases.

Our results are closely related to the investigations of Hiraoki & Ogawa [19] who investigated the mode interaction at small subcriticality, and proved through rigorous numerics the existence of the even-symmetric branch of localised states. The results presented in this paper shed light on those aspects of homoclinic snaking that should be expected to persist in a finite domain, and provide a different perspective on the formation and structure of localised states, as arising from mode interactions between periodic patterns; this is complementary to their usual interpretation as homoclinic orbits arising in a heteroclinic tangle for the spatial dynamical system obtained by considering steady solutions of fourth-order reversible PDEs such as (1.1).

Investigations along similar lines for the Swift–Hohenberg equation with a 'quadratic-cubic' nonlinearity by Bergeon et al. [6] and reveal more intricate connections and reconnections of the snaking curves due to variations in the localised pattern wavelength along the snake. For example this leads in some cases to the top and bottom

ends of the snake connecting to different periodic pattern branches; this arises also in the 'slanted snaking' problem analysed in [16] and can be observed in figures 6 and 8 of that paper. Further features of the quadratic-cubic case on a finite domain with Robin boundary conditions $w_{xxx} = 0$ and $w_x = \pm\beta w$ at $x = 0, L$ are discussed by Houghton & Knobloch [20].

**Acknowledgements.** The author would like to thank Edgar Knobloch for bringing ref. [19] to his attention, and John Burke for useful discussions. This work was begun during the 2005 programme *Pattern Formation in Large Domains* at the Isaac Newton Institute, Cambridge, UK. JHPD was supported by Newnham College, Cambridge when part of this work was carried out, and he currently holds a Royal Society University Research Fellowship.

REFERENCES

[1] N. Akhmediev and A. Ankiewicz (eds) 2005 *Dissipative Solitons*. Lect. Notes in Physics **661**. Springer, Berlin.
[2] O. Batiste and E. Knobloch 2005a Simulations of oscillatory convection in $^3$He – $^4$He mixtures in moderate aspect ratio containers. *Phys. Fluids* **17** 064102
[3] O. Batiste and E. Knobloch 2005b Simulations of localized states of stationary convection in $^3$He – $^4$He mixtures. *Phys. Rev. Lett.* **95** 244501
[4] M. Beck, J. Knobloch, D. Lloyd, B. Sandstede and T. Wagenknecht 2008 Snakes, ladders and isolas of localised patterns. Preprint.
[5] D. Bensimon, B.I. Shraiman and V. Croquette 1988 Nonadiabatic effects in convection. *Phys. Rev.* A **38** 5461–5463
[6] A. Bergeon, J. Burke, E. Knobloch & I. Mercader 2008 Eckhaus instability and homoclinic snaking. *Phys. Rev.* E **78** 046201
[7] U. Bortolozzo, M.G. Clerc, C. Falcon, S. Residori and R. Rojas 2006 Localized states in bistable pattern-forming systems. *Phys. Rev. Lett.* **96**, 214501
[8] C.J. Budd, G.W. Hunt and R. Kuske 2001 Asymptotics of cellular buckling close to the Maxwell load. *Proc. Roy. Soc. Lond.* **457**, 2935–2964
[9] J. Burke 2008 PhD thesis, University of California at Berkeley.
[10] J. Burke 2008 Personal communication.
[11] J. Burke and E. Knobloch 2006 Localized states in the generalized Swift–Hohenberg equation. *Phys. Rev.* E **73**, 056211
[12] J. Burke and E. Knobloch 2007 Snakes and ladders: localized states in the Swift–Hohenberg equation. *Phys. Lett.* A **360**, 681–688
[13] S.J. Chapman and G. Kozyreff 2009 Exponential asymptotics of localised patterns and snaking bifurcation diagrams. *Physica* D **238**, 319–354
[14] P. Coullet, C. Riera and C. Tresser 2000 Stable static localized structures in one dimension. *Phys. Rev. Lett.* **84**, 3069–3072
[15] J.H.P. Dawes 2007 Localized states in thermal convection with an imposed vertical magnetic field. *J. Fluid Mech.* **570**, 385–406
[16] J.H.P. Dawes 2008 Localised pattern formation with a large-scale mode: slanted snaking. *SIAM J. Appl. Dyn. Syst.* **7**, 186–206
[17] E. J. Doedel 2007 AUTO07p: continuation and bifurcation software for ordinary differential equations. Technical report, Concordia University.
[18] M. Golubitsky, I.N. Stewart & D.G. Schaeffer, *Singularities and Groups in Bifurcation Theory. Volume II*. Springer, Applied Mathematical Sciences Series **69** (1988)
[19] Y. Hiraoka and T. Ogawa Rigorous numerics for localized patterns to the quintic Swift–Hohenberg equation. *Japan J. Ind. Appl. Math.* **22**, 57–75 (2005)
[20] S.M. Houghton and E. Knobloch 2009 Homoclinic snaking in bounded domains. Preprint.
[21] G.W. Hunt, M.A. Peletier, A.R. Champneys, P.D. Woods, M. Ahmer Wadee, C.J. Budd and G.J. Lord 2000 Cellular buckling in long structures. *Nonlinear Dynamics* **21**, 3–29
[22] G. Iooss and M.-C. Perouème 1993 Periodic homoclinic solutions in reversible 1 : 1 resonance vector fields. *J. Diff. Eq.* **102**, 62–88
[23] E. Knobloch 2008 Spatially localized structures in dissipative systems: open problems. *Nonlinearity* **21**, T45–T60

[24] G. Kozyreff and S.J. Chapman 2006 Asymptotics of large bound states of localized structures. *Phys. Rev. Lett.* **97**, 044502
[25] D.J.B. Lloyd, B. Sandstede, D. Avitabile and A.R. Champneys 2008 Localized hexagon patterns of the planar Swift–Hohenberg equation. *SIAM J. Appl. Dyn. Syst.* **7**, 1049
[26] D. Lloyd & B. Sandstede 2009 Localized radial solutions of the Swift–Hohenberg equation. *Nonlinearity* **22**, 485–524
[27] B.A. Malomed, A.A. Nepomnyashchy and M.I. Tribelski 1990 Domain boundaries in convection patterns. *Phys. Rev. A* **42**, 7244–7263
[28] F. Merkt, R.D. Deegan, D. Goldman, E. Rericha and H.L. Swinney 2004 Persistent holes in a fluid. *Phys. Rev. Lett.* **98**, 184501
[29] Y. Pomeau Front motion, metastability and subcritical bifurcations in hydrodynamics. *Physica* D **23** 3–11 (1986)
[30] J.D.M. Rademacher, B. Sandstede and A. Scheel 2007 Computing absolute and essential spectra using continuation. *Physica* D **229**, 166–183
[31] R. Richter and I.V. Barashenkov 2005 Two-dimensional solitons in the surface of magnetic fluids. *Phys. Rev. Lett.* **94** 184503
[32] H. Riecke 1999 Localized structures in pattern-forming systems. In *Pattern Formation in Continuous and Coupled Systems: A Survey Volume*. IMA Volumes in Mathematics and its Applications **115**, eds M. Golubitsky, D. Luss and S.H. Strogatz. Springer, New York, 215–229
[33] H. Riecke and G.D. Granzow 1999 Localization of waves without bistability: worms in nematic electroconvection. *Phys. Rev. Lett.* **81** 333–336
[34] H. Sakaguchi & H.R. Brand 1996 Stable localized solutions of arbitrary length for the quintic Swift–Hohenberg equation. *Physica* D **97**, 274–285
[35] C. Strümpel, H.-G. Purwins and Y.A. Astrov 2001 Spatiotemporal filamentary patterns in a dc-driven planar gas discharge system. *Phys. Rev.* E **63** 026409
[36] L.S. Tuckerman & D. Barkley Bifurcation analysis of the Eckhaus instability. *Physica* D **46** 57–86
[37] A.G. Vladimirov, J.M. McSloy, D.V. Skryabin and W.J. Firth 2002 Two-dimensional clusters of solitary structures in driven optical cavities. *Phys. Rev.* E **65** 046606
[38] P.D. Woods and A.R. Champneys 1999 Heteroclinic tangles and homoclinic snaking in the unfolding of a degenerate reversible Hamiltonian–Hopf bifurcation. *Physica* D **129**, 147–170